Cement and Concrete Composites 129 (2022) 104468

Contents lists available at ScienceDirect

Cement and Concrete Composites

journal homepage: www.elsevier.com/locate/cemconcomp

Effects of ladle slag on Class F fly ash geopolymer: Reaction mechanism and high temperature behavior

Y. Luo [a], K.M. Klima [a], H.J.H. Brouwers [a], Qingliang Yu [a,b,*]

[a] Department of the Built Environment, Eindhoven University of Technology, P.O. Box 513, 5600MB, Eindhoven, the Netherlands
[b] School of Civil Engineering, Wuhan University, 430072, Wuhan, PR China

ARTICLE INFO

Keywords:
Ladle slag
Alkali activation
Hybrid binder
Conversion
Elevated temperature

ABSTRACT

Due to its low hydraulic reactivity, ladle slag is currently underutilized with nearly 80% of annual generation is either landfilled or dumped. This work investigates the joint activation of LS with Class F fly ash, and the impact of ladle slag on fly ash geopolymer with the focus on activation, hydrates assemblage, conversion process, and thermal behavior. Results reveal that the unique reaction process of ladle slag in alkali activation system shows a positive influence on fly ash geopolymers. Within an alkaline system rich in soluble Si, the initially hydrated CAH phases transform into C-A-S-H, which not only hinders the conversion and enhances the mechanical strength but also retains the geopolymerization. The hybrid geopolymer system exhibits superior thermal performance to pure fly ash geopolymers, especially under high temperature exposure. With increasing ladle slag substitution, more stable crystalline phases are formed at high temperatures. After 800 °C exposure, a high residual compressive strength of 64.7 MPa is achieved with 25 wt% ladle slag addition compared to 55.2 MPa in pure fly ash geopolymers.

1. Introduction

Fire breakout remains a threat to building structures regardless the decades of improvement on passive fire prevention. As the most widely used construction material, Ordinary Portland Cement (OPC) is prone to structural distortion and mechanical deterioration at high temperatures owing to the thermal decomposition of calcium silicate hydrate and portlandite [1,2]. In the last decades, geopolymer has emerged as a promising fire-resistant binder over OPC. In general, the formation of geopolymer is involved in the reaction of alkali activators with aluminosilicate sources, such as fly ash (FA) and metakaolin [3]. With its typical three-dimensional aluminosilicate networks, geopolymer exhibits superior mechanical performance and structural integrity under high temperatures [4]. Nevertheless, in order to break through limitations such as energy-consuming high temperature curing and unsatisfied mechanical strength, attention has been increasingly drawn into blended alkaline systems for geopolymer nowadays. By incorporating a calcium source, mostly, granulated blast furnace slag (GGBFS), into aluminosilicates, a hybrid gel system can be obtained with modified characteristics [5–7]. The presence of soluble calcium leads to the formation of C-(A)-S-H gel and thus the mechanical strength can be largely improved. However, the thermal stability of alkali activated FA/GGBFS blends is relatively low compared to sole alkali activated FA, and inevitable decomposition and strength deterioration take place after exposure to high temperature [8–10].

As a by-product from the steelmaking industry, Ladle Slag (LS) represents about one-third of the total amount of slag produced in an electric arc furnace [11], and the annual production is estimated to be about 1.9–2.4 million tons annually in Europe [12]. Unfortunately, LS has attracted less attention as compared to its counterparts such as GGBFS and basic oxygen furnace slag (BOFS). It is reported that about 80% of LS production in Europe is either landfilled or in store yard [13], and the valorization of LS is extremely low. The further application of LS is largely hindered by its high degree of crystallinity and low Si/Al ratio due to the high basicity and slow cooling procedures in the furnace [14]. Thus, the joint activation of LS with aluminosilicate sources is proposed as an alternative approach to recycle LS as sustainable building materials. For instance, Bignozzi et al. [15] observed that LS partially participated in gel formation when substituting metakaolin, resulting in the coexistence of different types of gels and un-soluble crystalline phases dispersed in the matrix. However, one drawback of utilizing LS as cementitious material is the conversion reaction of calcium aluminate

* Corresponding author. Department of the Built Environment, Eindhoven University of Technology, P.O. Box 513, 5600MB, Eindhoven, the Netherlands.
E-mail address: q.yu@bwk.tue.nl (Q. Yu).

https://doi.org/10.1016/j.cemconcomp.2022.104468
Received 3 January 2022; Received in revised form 27 February 2022; Accepted 28 February 2022
Available online 8 March 2022

hydrate. The initially formed calcium aluminate hydrates such as CAH_{10}, C_2AH_8, are known to be metastable and will convert into a more stable phase C_3AH_6, which is accompanied by volume shrinkage and strength loss during the engineering application [16,17]. Therefore, to recycle LS as a supplementary cementitious material (SCM) in geopolymer system for the in-situ application, the conversion reaction must be controlled. Nevertheless, information related to the hydration reaction of LS within alkaline environment is still very limited, and the mechanism behind the conversion process of LS based geopolymers remains unknown.

From the perspective of phase composition and hydration process, LS is comparable to calcium aluminate cement (CAC). As the most important hydraulic binder used for refractory castable and concretes, CAC and its hydration products contain thermally stable crystalline phases at ambient conditions and form more stable compounds at high temperatures [18,19], which equips CAC with superior thermal stability over OPC. But, owing to its low annual production, CAC is considerably four or five times more expensive than OPC that largely raises its application cost [20]. Here, the similarities between LS and CAC in mineralogy and hydration reaction offer great potential for LS to replace CAC and therefore provide a sustainable and cost-efficient way to recycle LS for high temperature applications. However, the information concerning the thermal behavior of alkali activated LS is very limited. Adesanya et al. [21] reported that alkali activated LS based mortar shows comparable thermal performance to CAC under high temperatures, and their thermal behavior such as cracking, volume change, and residual strength is mainly influenced by the hydrated gels. Murri et al. [22] further investigated the thermal behavior of LS blended geopolymer in early-age (7 days) and revealed that the high calcium content and the presence of crystalline phase in LS has a strong influence on the final products after calcination. However, up to now, the long-term influence of LS, especially its typical composition in crystalline phases as well as the conversion reaction between calcium aluminate hydrates, on hydrate assemblage within hybrid geopolymer system is unclear. Moreover, how the resultant hydrate assemblage affects the thermal behavior of hybrid geopolymer deserves further investigation.

The main objective of this study is to investigate the reaction and conversion mechanisms of LS within a hybrid geopolymer system and the possibility of utilizing LS as SCM in FA based geopolymers for high temperature applications. The applied slag is directly collected from slag yard in the present study and the reactivity of the weathered LS is determined by an alkaline reactivity test. The LS substitution is ranged from 0 wt% to 25 wt% based on the preliminary investigation, and the related influence on the reaction kinetics, phase assemblage, conversion mechanism, microstructural and mechanical properties are investigated by a multiple analytical approach, applying calorimetric measurements, quantitative X-ray diffractometry (XRD), thermogravimetric analysis (TGA), Fourier transform infrared spectroscopy (FT-IR), porosimetry (MIP), micro-computed tomography (micro-CT) and mechanical strength testing. Moreover, high temperature exposure tests (400 and 800 °C) are performed to investigate the phase transformation, structural change, and mechanical strength evolution under high temperatures.

2. Experimental design

2.1. Materials

Low calcium (Class F) fly ash (FA) and ladle slag (LS) was used as raw materials in this work. FA was commercially purchased from Vliegasunie, The Netherlands. LS was provided by TATA Steel, The Netherlands, and the slag was collected directly from stockpiles. The received LS was processed using a disk mill to achieve the desired particle size. The particle size distribution of raw materials was determined by a laser particle size analyzer (Mastersizer 2000, Malvern Instruments, UK), as shown in Fig. 1. The average particle size (d50) of FA and LS were approximately 21.48 μm and 15.22 μm, respectively. The chemical composition was analyzed by X-ray fluorescence spectrometry (XRF) (PANalytical Epsilon 3) and the loss on ignition was determined by the mass difference from 105 °C to 1000 °C. The detailed chemical composition and the loss on ignition of FA and LS are given in Table 1. Sodium hydroxide pellets (analytical level of 99 wt.%) and commercial sodium silicate solution (27.69 wt% SiO_2, 8.39 wt% Na_2O, 63.9 wt% H_2O) were applied to prepare alkali activating solution. Distilled water was used to obtain a certain water/binder ratio.

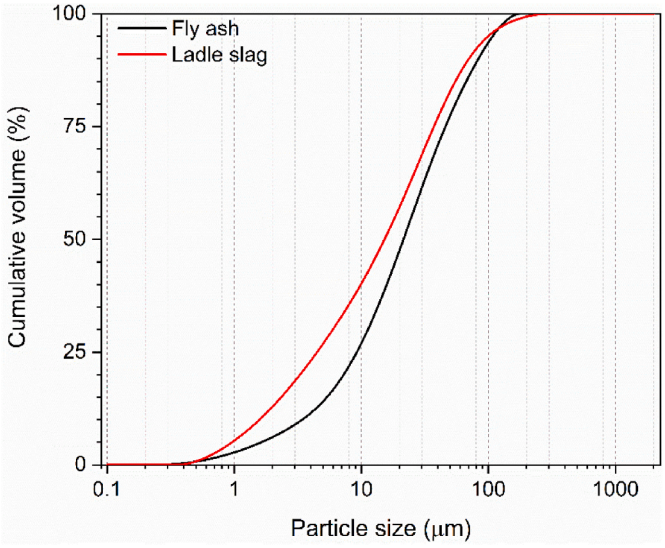

Fig. 1. The particle size distribution of raw materials.

2.2. Sample preparation

Alkali activator with desired silicate modulus (Ms, SiO_2/Na_2O molecular ratio) and equivalent Na_2O% was prepared by mixing a specific amount of sodium hydroxide pellets, sodium silicate solution, and distilled water. The pH value of the alkaline solution was about 13.15 ± 0.30. The obtained solution was kept at room temperature for 24 h prior to being used for geopolymer preparation. The detailed mix proportions are listed in Table 2. The added LS relative to binder (LS and FA) of 5, 15, and 25 wt% in mass were used (denoted by FL5, FL15, FL25, respectively) and a control sample without LS was also prepared (denoted by Ref.). In order to study the influence of LS addition on blended system individually, the silicate modulus, as well as the equivalent Na_2O%, were set constant as 1.5 and 6 wt% respectively for all samples. The mass ratio of water to binder was 0.35 in all pastes, in which the calculated water content consists of the added distilled water and the water in sodium silicate solution. In particular, the applied activator modulus, equivalent Na_2O%, and water to binder ratio were determined preliminarily to provide sufficient alkalinity with acceptable flowability, as well as to ensure good structural integrity after high temperature exposure for further characterization.

All paste specimens were prepared in a 5-L Hobart mixer. At first, dried precursors with a specific mass ratio were mixed in the mixer for 60 s to reach a homogeneous state. Then, the alkali activator was slowly added while stirring. The mixture was stirred for 30 s at a low speed and another 60 s at a high speed. Afterward, the slurry pastes were immediately cast into molds in size of 40 × 40 × 160 mm^3 and slightly vibrated for 1 min. All the specimens were cured at 20 °C under sealed condition for 24 h, followed by a 60 °C curing for another 24 h. After that, paste samples were demolded and sealed for 26 days at room temperature (20 °C) until further characterization.

Table 1
Chemical composition (wt.%) and loss on ignition of ladle slag and Class F fly ash.

Oxide	SiO_2	Al_2O_3	CaO	Fe_2O_3	MgO	SO_3	K_2O	Others	LOI (1000 °C)
Ladle slag	2.46	28.83	51.86	2.60	3.34	0.89	–	0.85	9.17
Fly ash	52.47	26.22	5.42	7.83	1.09	0.38	1.49	2.54	2.56

Table 2
Mix proportions and flowability of the investigated samples.

Sample code	LS/(FA + LS) (wt.%)	Ms	Na (wt.%)	w/b	Flowability (mm)
Ref.	0	1.5	6	0.35	308
FL5	5	1.5	6	0.35	293
FL15	15	1.5	6	0.35	268
FL25	25	1.5	6	0.35	212

2.3. Methodology

The flowability of the pastes was evaluated using the flow table tests according to EN 1015–3 [23]. A Hägermann cone (base diameter: 100 mm, top diameter: 70 mm, height: 50 mm) was applied for the slump flow test. The fresh pastes were transferred into the cone and then allowed to spread freely for 1 min. Two perpendicular diameters of each spread were measured, and the average value was adopted (Table 2).

The reactivity test was performed on dry ladle slag. To provide a sufficient environmental alkalinity, an 8 M NaOH solution was applied according to prior studies [24,25]. The applied ladle slag powder was mixed with NaOH solution at a liquid-to-solid ratio of 50 in polyethylene bottles. Then, the sealed bottle was shaken by using a liner reciprocating universal shaker (SM-30, Edmund Bühler) for 24 h at a constant rate of 250 rpm. The residual was filtered with 0.45 μm paper and dried at 40 °C for 24 h before XRD test.

The isothermal calorimetry analysis was performed applying an isothermal calorimeter (TAM Air, Thermometric), and the heat release of the initial 7 days hydration was determined under a constant temperature of 20 °C. A certain amount of solid materials was firstly mixed with the alkali activator in the ampoule for 1 min to reach a homogenous paste, which was then immediately loaded into the calorimeter.

Thermogravimetry/differential scanning calorimetry (TG/DSC) analysis was conducted employing a Jupiter STA 449 F1 Netzsch instrument. The grinded powder samples were heated up to 1000 °C at a heating rate of 10 °C/min with nitrogen as the carrier gas.

The Fourier transform infrared spectroscopy (FT-IR) spectrum of samples was collected using a Varian 3100 instrument. All samples were scanned 20 times with the wavenumber ranging from 4000 to 400 cm^{-1} at a resolution of 1 cm^{-1}.

X-ray diffraction characterization was performed to alkali activated pastes before and after high temperature exposure with a Bruker D4 PHASER equipped with a LynxEye detector and Co X-ray tube for determining the mineralogical phases. The parameters were set as time 0.6 s, with the increment of 0.02, scanning range from 15° to 60°. For the qualitative study, all the test samples were grinded by ball milling before the test (<300 μm). Rietveld method was applied for the quantitative study. Silicon of 10 wt% was used as an internal standard, and the test samples were milled in an XRD-Mill McMrone for 15 min. The data analyses were performed applying TOPAS Academic software v5.0. The crystal structural data used for the qualitative and quantitative XRD analysis are provided in Table 3. For TG/DSC, FT-IR, and XRD analyses, the tested samples at certain ages (7, 28, and 56 days) were crashed and immersed in isopropanol for 7 days to cease hydration, and then dried at 40 °C for 24 h prior to further characterization.

To observe the pore structure of the obtained samples, mercury intrusion porosimetry (MIP) analysis was performed using a mercury porosimeter (AutoPore IV 9500, Micromeritics). Before MIP characterization, all tested samples were prepared to be cubic pieces with grain sizes between 2 and 4 mm. For the tested samples at the age of 28 days, the obtained pieces were immersed in isopropanol for 7 days and dried at 40 °C for further test, while the thermally treated samples were tested directly.

Table 3
Structural data of the phases used for XRD analysis.

Mineral compound	#PDF-reference	ICSD
Tricalcium aluminate (C_3A)	00-038-1429	1841
Mayenite ($C_{12}A_7$)	00-048-1882	62040
Dicalcium silicate (C_2S)	00-036-0642	81097
Katoite (C_3AH_6)	00-024-0217	9272
Nordstrandite ($Al(OH)_3$)	00-018-0050	34393
Hydrotalcite ($Mg_{0.667}Al_{0.333}$) $(OH)_2(CO_3)_{0.167}(H_2O)_{0.5}$	01-089-0460	81963
Periclase (MgO)	01-071-1176	64928
Calcite ($CaCO_3$)	01-077-2376	40544
Portlandite ($Ca(OH)_2$)	01-087-0673	15471
Magnetite (Fe_3O_4)	01-089-0951	31156
Hematite (Fe_2O_3)	01-089-2810	22505
Quartz (SiO_2)	01-083-0539	83849
Mullite ($Al_{1.69}Si_{1.22}O_{4.85}$)	01-089-2813	43297
Nepheline ($(Na, K)AlSiO_4$)	01-085-1487	26007
Wollastonite ($CaSiO_3$)	01-076-0186	23567
Gehlenite ($Ca_2Al_2SiO_7$)	01-089-1489	67687
Akermanite ($Al_{0.41}Ca_{1.53}Fe_{0.16}Mg_{0.39}Na_{0.51}O_7Si_2$)	01-072-2127	20391
Calcium sodium cyclo-hexaaluminate ($Ca_{8.5}NaAl_6O_{18}$)	00-026-0958	1880

Micro-CT 100 (Scanco Medical AG, Switzerland) was used for the tomographic scan on cut specimens (1 × 1 × 4 cm^3). The energy of X-rays for all the samples was fixed at 70 kV and 200 mA, and the pixel resolution for all samples was 10 μm. Tomographic reconstruction was performed using a stack of 205 slices to obtain a 3D visualization. With a 2048 × 2048 picture resolution, a software for 3D-image processing was employed for pore segmentation and internal structure visualization.

The compressive strength of obtained specimens at 7, 28, and 56 days were determined according to EN 196–1 [26]. Pastes were sealed with plastic foil and cured at ambient temperature until the testing age. A loading rate of 2400 N/s was applied, and the recorded strength value was obtained from the average of 3 specimens.

According to the domain factors (dehydration, recrystallization, sintering) that govern the high temperature behavior of fly ash based AAMs, two target temperatures, i.e., 400 °C, 800 °C, were chosen to investigate the thermal behavior of the obtained specimens. 28 days cured pastes were loaded in a high temperature oven with a heating rate of 10 °C/min from room temperature to the target temperature. All the specimens were kept at the target exposure temperature for 1 h to reach the thermal equilibrium state, and then gradually cooled down to ambient temperature in the oven. In avoiding moisture immersion, the thermally treated samples were sealed with plastic foil before further characterization.

The mass loss of samples under high temperature was determined by comparing the mass of the prismatic sample before and after the designed temperature exposure. The volume change was recorded based on the measurement of the three-dimensional size of prismatic samples before and after elevated temperature exposure. The bulk density was calculated according to the measured mass and volume of the specific specimen. Among these, the reported volume, mass, and density values were recorded as the average of three specimens.

3. Results

3.1. Characterization of raw materials

Ladle slag (LS) is produced in the final stage of steelmaking, in which the liquid steel is poured into a ladle furnace where it is deoxidized and desulphured under the protection of basic slag. In this stage, aluminium is used as the deoxidation agent, leading to the formation of calcium aluminates. It is known that calcium aluminates, especially mayenite ($C_{12}A_7$), are highly hydraulic, which would react with moisture [14]. The hydration products of calcium aluminates can be varied due to the nature of phases, according to the following [27,28]:

$$C_{12}A_7 + 51H \rightarrow 6C_2AH_8 + AH_3 \quad (1)$$

$$2C_3A + 21H \rightarrow C_4AH_{13} + C_2AH_8 \quad (2)$$

However, these initially formed calcium aluminate hydrates are known to be metastable and will convert into more stable phase C_3AH_6 through the endothermic reactions as shown in Eqs. (3) and (4) [16,29]:

$$3C_2AH_8 \rightarrow 2C_3AH_6 + AH_3 + 9H \quad (3)$$

$$C_4AH_{13} + C_2AH_8 \rightarrow 2C_3AH_6 + 9H \quad (4)$$

During the slag manufacturing in steel plant, a mist spray process is always adopted to either cool down the slag or dedusting, afterward, the slag is piled up in slag yard, waiting for further landfill disposal. After this process, the above reactions would have highly possibly occurred during weathering, which makes the composition of applied LS very complex.

According to XRD Rietveld results presented in Table 4, apart from the intrinsic phases of $C_{12}A_7$ (7.8 wt%), C_3A (34.2 wt%), and C_2S (6.6 wt %), abundant C_3AH_6 (18.5 wt%) is also observed. This confirms the hypothesis that the applied LS would react upon contacting with moisture, following Eqs. (1)–(4) [30]. Moreover, small traces of periclase, portlandite, hydrotalcite, and metallic iron are identified.

To determine the reactivity of weathered LS under alkaline environment, a reactivity test is carried out on as-received raw LS, as the LS powder is dissolved in alkaline solution for 24 h. The presence of hydrated calcium aluminates in raw LS and residue is compared by TG-DTG analysis, as shown in Fig. 2. For the raw LS, the slight mass loss peak at around 150 °C is associated with the dehydration of unconverted metastable phases such as CAH_{10}, C_2AH_8 [31,32], while the main weight loss peak shown at around 300 °C is attributed to the dehydration of C_3AH_6 [32–34]. It therefore can be concluded that, during weathering, most metastable hydrates such as CAH_{10}, C_2AH_8 in LS are converted into stable phase C_3AH_6 following Eqs. (3) and (4). The small shoulders observed in 224 °C and 370 °C could be the decomposition of hydrotalcite [35,36]. The mass loss peak centered at around 450 °C corresponds to the decomposition of portlandite. In addition, insignificant

Table 4
The mineralogical composition of ladle slag acquired with Rietveld refinement.

Mineral compound	Chemical formula	Content (wt. %)
Tricalcium aluminate (C_3A)	$Ca_3Al_2O_6$	34.2 ± 0.4
Mayenite ($C_{12}A_7$)	$Ca_{12}Al_{14}O_{33}$	7.8 ± 0.2
Dicalcium silicate (C_2S)	Ca_2SiO_4	6.6 ± 0.4
Katoite-hydrogarnet (C_3AH_6)	$Ca_3Al_2(O_4H_4)_3$	18.5 ± 0.2
Nordstrandite ($Al(OH)_3$)	$Al(OH)_3$	0.6 ± 0.2
Hydrotalcite	$(Mg_{0.667}Al_{0.333})(OH)_2(CO_3)_{0.167}(H_2O)_{0.5}$	0.7 ± 0.1
Periclase (MgO)	MgO	2.5 ± 0.1
Portlandite ($Ca(OH)_2$)	$Ca(OH)_2$	1.3 ± 0.1
Metallic iron (Fe)	Fe	0.4 ± 0.1
Amorphous	–	27.3 ± 0.9

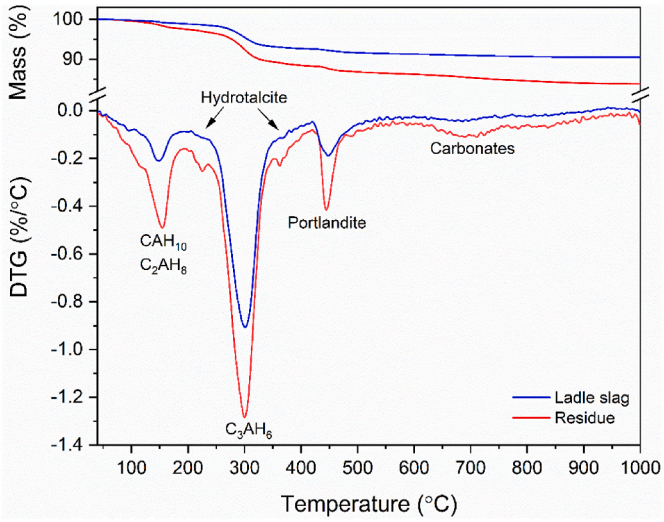

Fig. 2. TG-DTG analysis of raw ladle slag.

weight loss peaks at approximately 680 °C and 800 °C should be assigned to the decomposition of carbonates and dehydration of $C_{12}A_7H$, respectively [30]. By contrast, a higher mass loss is detected for the residue LS after 8 M NaOH treatment. It is interesting to note that both the mass loss peak intensity of metastable and stable phases are increased. However, since part of metastable phases would transform into C_3AH_6 at around 150 °C, resulting in the increase of C_3AH_6 peak intensity [37], which makes it difficult to identify the formation of C_3AH_6.

In Fig. 3, the XRD results of the residual LS are compared with the raw LS. The crystalline patterns present in the residue LS remain the same as compared to the raw LS, while the intensity of typical phases varies. The calcium aluminates in LS, namely, $C_{12}A_7$ and C_3A, are largely dissolved after NaOH treatment, and the intensity of C_3AH_6 appear to increase in the residue LS. Nevertheless, no metastable phases such as CAH_{10} and C_2AH_8 are observed in XRD, which might be due to their low content or poor crystallinity. Thus, it is confirmed by combining the discussion above that the co-existence of metastable and stable phases in alkali-treated LS. This is in line with previous studies on CAC system that during the hydration of calcium aluminates, the conversion between metastable hydrates to stable C_3AH_6 is expedited under a moderately

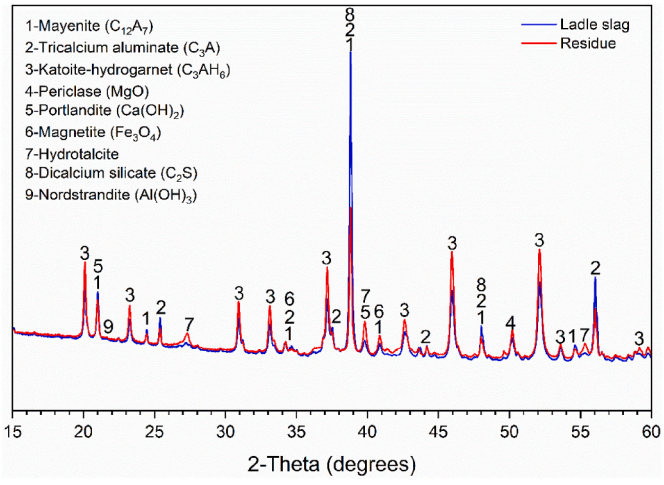

Fig. 3. XRD patterns of raw ladle slag and residue ladle slag after 8 M NaOH treatment (Legend: 1-Mayenite, 2-Tricalcium aluminate, 3-Katoite-hydrogarnet, 4-Periclase, 5-Portlandite, 6-Magnetite, 7-Hydrotalcite, 8-Dicalcium silicate, 9-Nordstrandite).

alkaline environment (usually the alkali concentration around 8 M) [38,39]. It can be concluded that the conversion reaction of LS occurs within 24 h in an 8 M NaOH environment. Moreover, the observed crystalline phases transformation from calcium aluminates to C_3AH_6 after alkaline treatment indicates that the applied LS still shows a certain degree of reactivity in the alkaline environment even after weathering.

3.2. Reaction kinetics

The influence of LS substitution on the reaction kinetics of hybrid system at the early stage is characterized by isothermal calorimetric analysis. In Fig. 4a, only one exothermic peak is detected at the early stage, which is ascribed to the dissolution of solid raw material, as well as the formation of the initial dissolved silicate units and their complexation with calcium and sodium [40]. During the test period, no other visible heat peak can be detected even with a higher dosage of LS. Such sole peak phenomenon has widely been reported for sole fly ash based alkali activated materials [41,42]. It can be deduced that, in the hybrid system, the sole exothermic peak is the combined effects of two phenomena: the late reaction of FA and the high reactivity of calcium aluminates in LS. On the one hand, as the main body of the mixture, the relatively slow dissolution of FA can result in a slow transformation of dissolved species into gels. As can be observed from Fig. 4b, the cumulative heat of all samples keeps increasing after the extensive exothermic heat flow, indicating the continuous dissolution and geopolymerization process, which is, however, not detectable in the heat flow curve. On the other hand, as suggested by Adolfsson et al. [14] that the dissolution and hydration of C_3A and $C_{12}A_7$ occur within 1 h, and therefore, the existence of sole peak might also be caused by the overlapping of solids dissolution and rapid hydration of LS.

In addition, by comparing the heat evolution curve of the sample with different LS substitutions, the hydration reaction is in general positively affected by LS addition. The higher the LS substitution, the larger the heat flow and cumulative heat. Here, one can conclude that a higher amount of LS promotes the dissolution process, which leads to an increase in heat flow peak intensity as well as cumulative heat release. Nevertheless, a very slight retardation effect is observed in the sample with the lowest LS addition. This can be due to the small amount of LS is insufficient to promote the reaction but further reduces the environment pH by releasing metal ions in the dissolution process. Furthermore, as widely accepted by other researchers [43], the flowability of AAMs is dependent on the dissolution and polymerization of precursors. As presented in Table 2, the flowability of mixtures in this work is strongly affected by LS addition that reduces with the increased amount of LS, which further confirms the influence of LS on reaction kinetics.

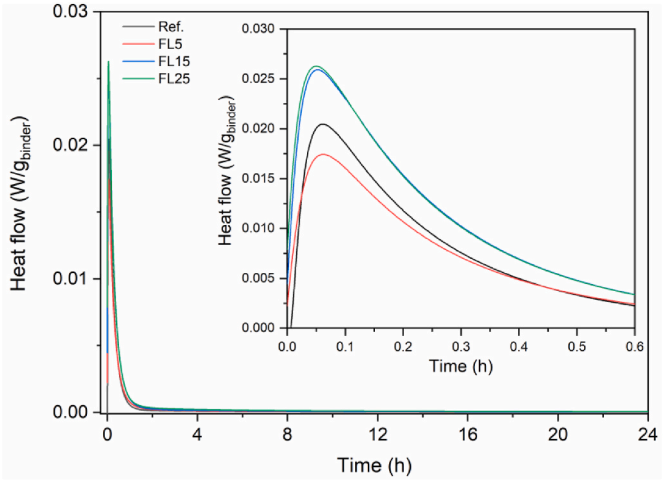

Fig. 4. Isothermal calorimetric response of FA/LS based geopolymer pastes at 20 °C a) normalized heat flow, and b) normalized cumulative heat.

3.3. Hydrates assemblage

Fig. 5 compares the XRD patterns of all samples at the age of 28 days. As for the Ref., crystalline phases including quartz, mullite, Fe_xO_y (magnetite and hematite), periclase, and calcite are observed. In XRD patterns of LS substituted samples, besides the phases observed in the Ref., traces of C_3A and C_3AH_6 are also detected. Meanwhile, with the increased addition of LS, the intensity of peaks ascribing to C_3A and C_3AH_6 are noticeably increased. As one of the main phases in LS, the increase in C_3A with more LS indicates C_3A cannot be fully consumed after 28 days of curing. While C_3AH_6 may not only be introduced by the applied weathered LS but also hydrated from $C_{12}A_7$ and C_3A. The Rietveld refinement results as shown in Fig. 13 will be discussed later.

FTIR is performed on raw material powder and hybrid pastes with different LS content. In Fig. 6a, three adsorption peaks are observed for raw FA, where the major band at around 1046 cm^{-1} corresponds to the asymmetric stretching vibration of Si–*O*-T bonds (T represents Si or Al units) [44], the broad peak at 670-850 cm^{-1} represents the stretching vibrations of Si–*O*–Si in quartz and the weak peak at 1450 cm^{-1} attributed to the stretching vibrations of O–C–O bonds might result from

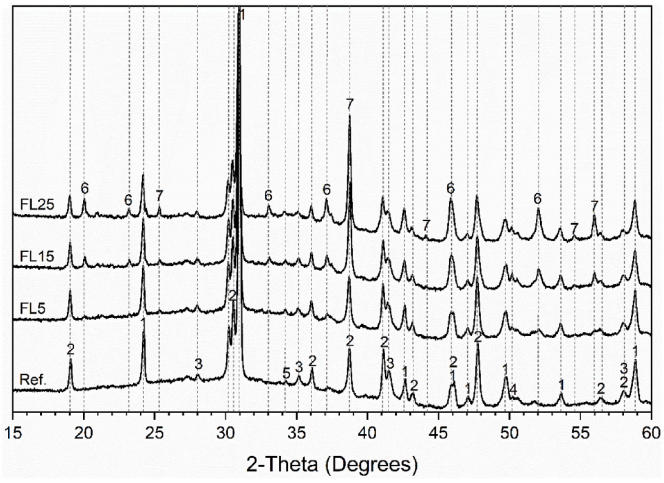

Fig. 5. XRD patterns of pastes prepared with different LS addition (Legend: 1-Quartz, 2-Mullite, 3-Iron oxides (Fe_xO_y), 4-Periclase (MgO), 5-Calcite ($CaCO_3$), 6-Hydrogarnet (C_3AH_6), 7-Tricalcium aluminate (C_3A)).

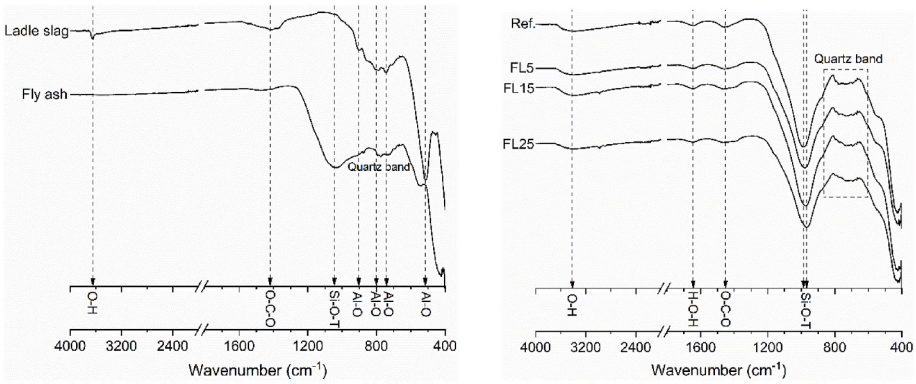

Fig. 6. FTIR spectra of (a) ladle slag and fly ash, (b) FL blends.

incomplete combustion of carbon. For raw LS, the sharp adsorption at approximately 3654 cm^{-1} is due to the O–H stretching vibrations of portlandite [30,45]. The intensive peak at 1415 cm^{-1} is related to O–C–O bonds of carbonates as also observed in TG (Fig. 2) [40]. The adsorption peak of 510 cm^{-1} corresponds to the vibrational peak in symmetric Al–*O*–Al and the adsorptions of 741, 798, 903 cm^{-1} are assigned to the stretching and bending vibrations of the Al–O bonds [46–48], indicating the presence of different calcium aluminates.

The infrared spectra for samples with different LS additions are shown in Fig. 6b. The broad adsorption band appearing at around 3415 cm^{-1} and the adsorption at around 1645 cm^{-1} are associated with the stretching vibrations of O–H bonds and bending vibrations of physically and chemically bond water. The adsorption peak of O–C–O bonds at 1452 cm^{-1} is observed in all spectrums, which could be associated with carbonates and the residual carbon in raw FA as noticed in Fig. 6a. The typical absorption band of the Si–*O*-T bridge bond in the Ref. shifts to a lower wavenumber as compared to pure FA due to the polymerization. Furthermore, it is interesting to note that, with more LS addition, the Si–*O*-T bond adsorption peak shifts from 990 cm^{-1} to 965 cm^{-1}, indicating the increased substitution of Al in Si–*O*-T tetrahedral within geopolymer gel [49,50]. In conclusion, with increasing LS substitution, more Al is introduced into geopolymeric gel and a higher degree of cross-linking is formed.

The difference in hydration products with varying LS addition is further reflected with thermogravimetric analysis, as shown in Fig. 7. In the Ref., the main mass loss peak below 120 °C is mainly due to the release of physically bound water [51]. A broad mass loss peak observed in the temperature range between 450 °C and 650 °C is associated with the combustion of unburned carbon in raw FA [52]. Furthermore, an insignificant weight loss peak that occurs after 800 °C is mainly induced by the re-crystallization reaction [53]. For the LS substituted sample, an additional weight loss peak that appears at around 300 °C can be assigned to the dehydration of C_3AH_6. In accordance with the XRD results, the C_3AH_6 typical peak is intensified as a higher dosage of LS is applied, indicating that more C_3AH_6 is introduced. The decomposition of carbonates is also observed at around 680 °C.

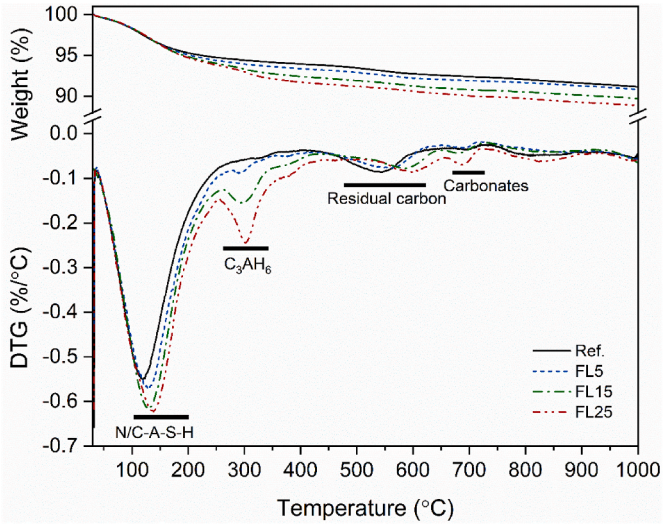

Fig. 7. Thermal analysis of pastes with different LS addition.

Moreover, it should be noted that, as the LS addition increases, the main mass loss peak is intensified and the corresponding peak shifts towards higher temperatures. This might be attributed to the higher amount of hydration gel with more tightly bound water and/or smaller pores are formed in the hybrid system [54]. On the one hand, with LS substitution, additional calcium aluminate hydrates are formed as discussed above. On the other hand, as evidenced by Fernández-Jiménez et al. [55] on calcium aluminate cement (CAC) system with the presence of silica, Si can be taken in CAH phases into C-A-S-H phase. In this work, the soluble silica provided by fly ash as well as sodium silicate can promote the formation of C-A-S-H phase. Here, metastable phases from LS dehydrate at a range from 120 to 195 °C [33], and C-A-S-H gradually dehydrates at about 160 °C [6], hence the dehydration of these hydration products occurs within a similar range between 100 °C and 200 °C, which overlaps the main weight loss peak, making the change in C-A-S-H content not observable on the DTG curves. Nevertheless, a clear difference in peak intensity and corresponding temperature can be observed, indicating more aluminosilicate species are introduced with higher LS substitutions.

3.4. Microstructural properties

The pore structure of 28 days pastes with different substitutions of LS is investigated via Mercury intrusion porosimetry (MIP) as depicted in Fig. 8. The detailed characteristic pore parameters are summarized in Table 5, including mesopores (2–50 nm), macropores (>50 nm), open porosity, median/average pore diameter, and intrusion volume of mercury. In Fig. 8a, for all tested samples, most of pores are concentrated in the range of 5–1000 nm, while a very small fraction of pore larger than 100 μm is also detected, which reflects the presence of entrained air voids and pre-existing microcracks.

In terms of total porosity, it must be noted that, with LS substituting up to 25 wt%, the porosity remains almost unchanged and only slightly varies between 38.9% and 40.4% are observed. This indicates that LS has a very limited influence on porosity within the present substitution level. According to the pore type, the pores are further classified into 3

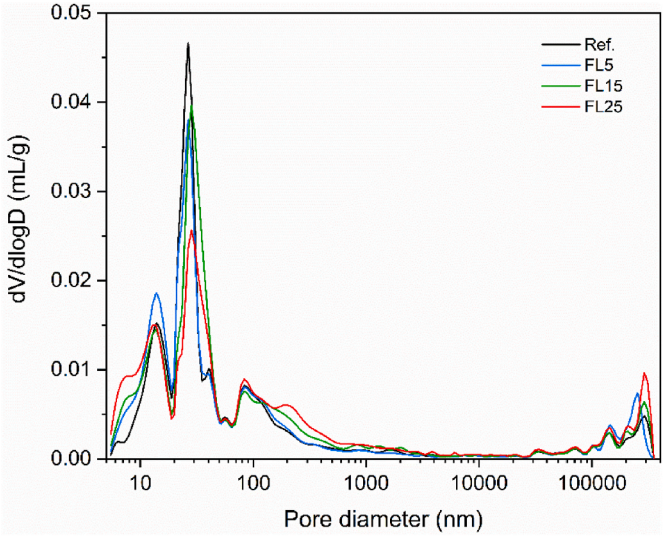

(a)

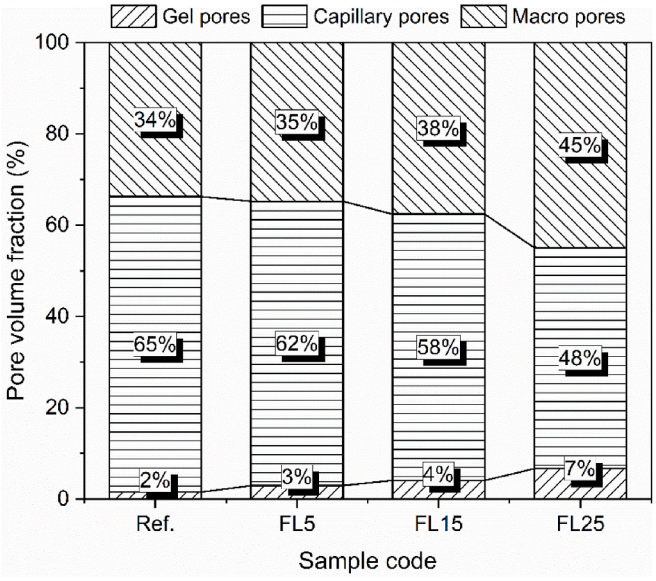

(b)

Fig. 8. MIP results of pastes after 28 days of hydration, a) pore size distributions, and b) pore volume fractions.

types: gel pores (≤10 nm), capillary pores (10–50 nm), and macropores (>50 nm) [56], and the fractions of pores are shown in Fig. 8b. In agreement with previous works [15,22], the LS dosage strongly influences the pore size distribution (PSD) of the blended system. In this work, a clear trend is observed that the fraction of gel pores, as well as macropores, increase while that of capillary pores decreases with the LS addition rise from 0 to 25 wt%. It is widely accepted that the pore size reflects the reaction degree, and the well-reacted sample may exhibit the highest proportion of gel pores. Here, the increased fraction of gel pores further confirms the promotion of hydration by LS. While the higher macropores fraction with more LS addition should be partially attributed to the poor workability that entraps more air bubbles/voids in the matrix. On the other hand, as revealed by Choi et al. [57], the typical continuous plate-shape geometry of calcium aluminate hydrates would have a direct influence on the process of unreacted particle in contact with water, in consequence, macropore is more favourable to be formed.

3.5. Mechanical properties

The compressive strength of the samples with the substitution of LS varying from 0 to 25 wt% at different curing ages are evaluated and presented in Fig. 9. The compressive strength increases with LS substitution from 0 to 15 wt%, and then slightly declines. Here, as discussed in Section 3.3, the enhancement in compressive strength can be attributed to a higher degree of hydration with more LS substitution, which strengthens the matrix with higher content of hydrated gel. However, the slight strength reduction in FL25 might be induced by the change in the pore structure. It is suggested by Mehta et al. [58] that the mechanical strength is controlled by micropores, while macro pores larger than 50 nm would have an adverse effect on strength of the matrix. As learned by PSD in Fig. 8, FL25 has the highest macropore fraction, which will negatively impact the compressive strength.

Regarding the strength evolution of mixtures at different curing ages, all mixtures gain strength during the 56 days of curing, contradicting sole LS based materials, which are prone to lose strength between 7 and 28 days due to conversion reaction [14,31,59]. In this study, the strength enhancement during the tested curing ages, on the one hand, can be ascribed to the further hydration of unreacted raw materials. On the other hand, in accordance with the conversion mechanism revealed above, calcium aluminate hydrates that convert into stronger C-A-S-H gel with the available soluble silica source. Moreover, it is interesting to note that the strength development rate from 7 days to 56 days is decreased gradually with LS substituted from 5 wt% to 25 wt%. This observation indicates that since the environmental silica content is consumed or insufficient, the increasing C_3AH_6 content with a higher LS substitution would further have an adverse impact on strength gain during curing.

From the point of view of utilizing LS as SCM, the incorporation of LS

Table 5
Characteristic pore parameters of samples under different temperatures as measured by MIP.

Exposure temperature (°C)	Sample code	Porosity			Median pore diameter (nm)	Average pore diameter (nm)	Total intrusion volume (mL/g)
		Mesopores (2–50 nm)	Macropores (>50 nm)	Total			
20	Ref.	25.8	13.1	38.9	29.30	30.34	0.27
	FL5	26.4	14.0	40.4	28.88	28.28	0.28
	FL15	24.4	14.6	39.0	34.95	29.96	0.28
	FL25	21.5	17.4	38.9	39.88	28.73	0.27
400	Ref.	22.9	18.2	41.1	46.62	46.12	0.29
	FL5	25.9	14.9	40.8	39.11	40.66	0.28
	FL15	22.7	18.1	40.8	47.02	46.28	0.32
	FL25	20.4	21.1	41.5	51.19	49.25	0.27
800	Ref.	2.2	34.2	36.4	2161.88	208.14	0.24
	FL5	2.1	34.1	36.2	1914.17	211.63	0.23
	FL15	2.0	34.6	36.6	2506.22	237.13	0.24
	FL25	2.0	35.2	37.2	2720.18	276.50	0.24

Table 6
Structural characteristics of samples at different temperatures.

Sample code	Mass loss (%)			Bulk density (g/cm^3)			Volume shrinkage (%)		
	20 °C	400 °C	800 °C	20 °C	400 °C	800 °C	20 °C	400 °C	800 °C
Ref.	–	19.82	21.84	1.72	1.47	1.56	–	6.17	13.25
FL5	–	20.19	22.66	1.68	1.43	1.53	–	6.58	15.03
FL15	–	21.16	23.37	1.68	1.43	1.53	–	7.38	15.55
FL25	–	22.41	24.05	1.71	1.43	1.55	–	7.61	15.80

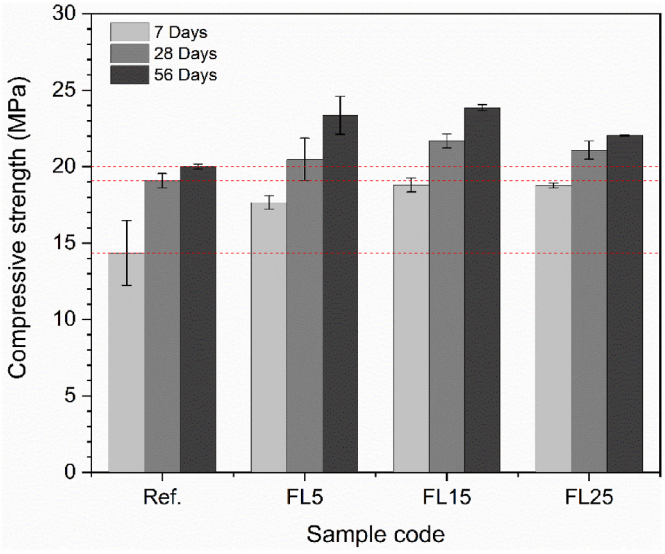

Fig. 9. Compressive strength of pastes with different LS dosage after 7, 28, and 56 days of hydration.

into hybrid alkaline system not only avoids strength loss, but also improves the mechanical strength as compared to sole FA based samples by forming C-A-S-H type gel. Moreover, the best mechanical performance is observed for the mixture with 15 wt% LS substitution.

3.6. Thermal behavior

Owing to the similarity in mineralogy and reaction mechanism, LS can be compared with CAC which is mainly applied in refractory castable/concrete and linings due to its outstanding thermal performance. In this study, the thermal behavior of LS as a SCM in geopolymer system is evaluated by applying high temperature exposure tests.

3.6.1. Structural change

The variations of structural properties of samples treated at different temperatures are given in Table 6. The main mass loss is observed before 400 °C in all samples, which is caused by the release of physically and chemically bound water. As a result, the density of all samples decreases due to the increased content of empty pores. At the same time, the loss of water leads to a range of capillary strain and shrinkage of pores, resulting in a volume shrinkage in all samples. In the temperature range between 400 °C and 800 °C, the slight mass loss is mainly associated with the decomposition of portlandite and carbonates of different crystallinity [60]. While the increase in density and volume shrinkage for all samples from 400 °C to 800 °C is owing to the viscous sintering that occurs at around 600 °C which leads to structural densification [61]. Regarding the influence of LS substitution on structural change, the densities of all samples are similar at the tested temperatures, whereas the higher the LS substitution, the severer the mass loss and higher volume shrinkage are detected at high temperatures. As evidenced by TG-DSC analysis (Fig. 7), the intensified mass loss with higher LS contents can be ascribed to the growth of hydration products. Further, it is noted that the increased volume shrinkage is not only induced by the greater water release but also the severer re-crystallization detected in LS substituted sample.

The pore structure evolution of samples upon high temperatures is characterized by MIP, as summarized in Table 5. The porosity in all samples is found to increase after exposure to 400 °C. Meanwhile, the fraction of mesopores is reduced while macropores are detected to increase. This can be explained by the pore collapse and cracking induced by the migration of both physical and chemical water towards the surface, which results in the formation of larger pores with increased pore interconnectivity. In the temperature range 400 °C–800 °C, the porosity is slightly decreased, among which, a remarkable reduction is detected in the fraction of mesopores, while macro pores fraction is largely increased. Here, the sintering reaction leads to the healing of micropores/cracks, which results in the decline of small pores [62]. In the meantime, more large cracks are formed due to the dehydration and decomposition of the matrix, which is detected as macropores in MIP.

It is known that MIP only measures connected open pores that are smaller than 350 μm. In order to visualize the pore structure and characterize the variation of pores in a larger coverage, Micro-CT analysis is carried out. To determine the effect of LS, FL15 with optimum hardened and thermal performance is selected as a representative sample to compare with Ref. for Micro-CT analysis. The pore structures are extracted and denoted in different colors according to pore size as shown in Fig. 10. By comparing the images of the Ref. and FL15, obviously, the substitution of LS introduces more big pores as compared to the Ref. at all temperatures. In addition, the detailed pore size distribution of samples upon high temperatures is presented in Fig. 11. It can be learned that the samples with and without LS substitution show a different pattern of pore size distribution. In Fig. 11a and d, the Ref. exhibits a narrow pore size distribution below 0.3 mm with a main peak centered around 0.05 mm, while a wide and even pore size distribution is observed in LS substituted sample. With the exposure temperature increases from 20 °C to 800 °C, in the Ref., the fraction of pores between 0 and 0.1 mm is largely increased, and bigger pores ranging from 0.4 to 0.5 mm are detected. Nevertheless, for LS substituted sample in Fig. 11b, d, and f, the pores below 0.3 mm are relatively stable at elevated temperatures, except more big pores at around 0.5 mm are detected. This can be explained by the wide and even distribution of pore size in the LS substituted sample that facilitates the release of inner water or gas vapour at elevated temperatures that reduces the internal damage induced by pore pressure. While the narrower pore size distribution with the main fraction range from 0 to 0.1 mm for the Ref. tends to generate higher pore pressure, leading to severer pore collapse and crack extension with the increased porosity. But relatively large cracks from 0.4 to 0.5 mm can be detected in both mixtures due to severe shrinkage. In conclusion, samples with LS substitution exhibit a better inner structural stability under elevated temperatures owing to the wide and even pore size distribution. This is believed to contribute to retain a large degree of strength under elevated temperatures.

3.6.2. Phase transformation

The phase transformation of samples at different temperatures is compared in Fig. 12. The loss of bound water (amorphous) due to high temperature exposure is excluded according to TG results. Because the contents of some crystalline phases such as periclase, rutile, etc., are

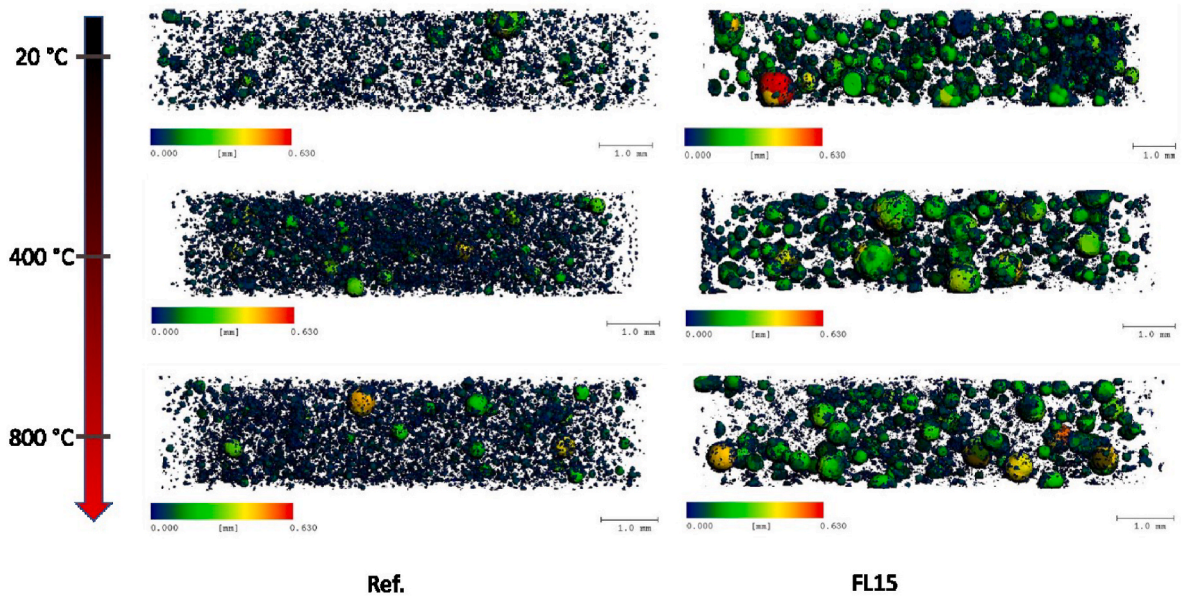

Fig. 10. Micro-CT images of the Ref. and FL15 at different temperatures.

relatively low and similar in different mixtures, which are not of comparison, they are classified as other phases (the detailed results from XRD-Rietveld are provided in Supplementary material).

It is clear that the crystalline phases in the Ref. are thermally stable at 400 °C, while the amorphous content decreases and a minor trace of nepheline appears up to 800 °C. This can be explained by the release of bound water and partial recrystallization of amorphous aluminosilicates, which has been reported in sole fly ash based geopolymer [4]. Regarding the sample with the addition of LS, obvious transformation can be observed at elevated temperatures. In accordance with TG results, hydrogarnet disappears after 400 °C exposure, and then, mayenite starts to appear. Moreover, the content of C_3A and mayenite increases with higher LS substitutions. It is worth noting that the phase change among LS substituted samples at 400 °C is mainly induced by the dehydration of hydrogarnet into calcium aluminates, and the total crystalline content almost remains unchanged, indicating that the hybrid gel system is relatively stable at 400 °C. After 800 °C exposure, it is obvious that the amorphous content decreases whereas the crystalline phase content increases with higher LS substitutions. New phases such as wollastonite, akermanite, and gehlenite are detected, and clearly, their contents are increased with more LS substitutions. Among these, it is known that wollastonite is highly associated with LS. Akermanite and gehlenite are formed by the crystallization of C-A-S-H gel [63], which correlates well with the phase assemblage discussed above that substitution of LS can promote the formation of C-A-S-H type gels in the hybrid system. Owing to the fact that Ca^{2+} could be replaced by Na^{+} in C_3A structure within a Na rich system, two structures including C_3A and Na^{+} substituted C_3A (Calcium Sodium Cyclo-hexaaluminate, $Ca_{8.5}NaAl_6O_{18}$) are adopted for the refinement, and their total content is similar to that of 400 °C. The increase in nepheline with more LS addition can be partially caused by the increasing Al ion from LS is taken up to form more sodium based aluminosilicate species [25]. In addition, the increasing C-A-S-H phase ascribed to the introduction of additional calcium from LS promotes the formation crystalline phases such as akermanite and gehlenite at 800 °C [64]. Thus, a higher crystalline phase content is detected with higher LS substitutions.

3.6.3. Thermal mechanical properties

Here, the changes in the porosity do not reflect the evolution of the mechanical strength of samples at high temperatures. This is because the thermal mechanical evolution of geopolymer based material is not only influenced by physical change but also chemical transformation during thermal exposure. As presented in Fig. 13, it is remarkable that the substitution of LS does not lead to strength deterioration at high temperatures as always experienced in other FA/slag systems and a continuous strength gain is observed. At 400 °C, the strength gain is mainly induced by further geopolymerization of unreacted fly ash. In this regard, the pure fly ash paste exhibits the highest compressive strength and strength gain among LS substituted samples. After being exposed to 800 °C, the strength gain observed in the sole fly ash sample is widely accepted to be caused by the sintering reaction of unreacted fly ash that heals the small cracks and densifies the matrix as learned above. While it should be noted that the residual strength at 800 °C is improved by LS substitution. The compressive strength, as well as the rate of strength gain increase with the LS substitution, rising from 15 wt% to 25 wt% compared to the Ref., and FL25 exhibits the highest compressive strength of 64.72 MPa after 800 °C exposure. Here, as observed in Table 6, the severer shrinkage and densification with more LS substitution can be considered as one of the contributing factors. On the other hand, it is revealed by Murri et al. [22] and Dombrowski et al. [64] that high temperature induced crystalline phases with different thermal stability can influence the thermal behavior of the matrix. In this work, as evidenced by Rietveld refinement, the crystalline phase content at 800 °C is increased with more LS substitution, among which, more stable phases including gehlenite, akermanite, C_3A, and mayenite are formed. It is therefore likely that these phases could act as stable aggregates that strengthen the matrix at high temperatures.

4. Discussion

4.1. The hydration mechanism of ladle slag within hybrid system

It is widely accepted that within an aqueous system, the hydration process can be divided into two stages: a) the hydration of LS with the initial metastable hydrates, dicalcium aluminate (C_2AH_8) before 7 days, b) the conversion from metastable phases into stable tricalcium aluminate hexahydrate (C_3AH_6) between 7 and 28 days, which is always accompanied with the increased porosity and reduced strength [31]. However, the hydration of calcium aluminates proceeds differently in an alkaline system. In KOH/Na_2SiO_4 activated LS system, Adesanya et al. [59] observed a clear reduction in compressive strength between 7 and 28 days, indicating the presence of conversion reaction in an alkaline

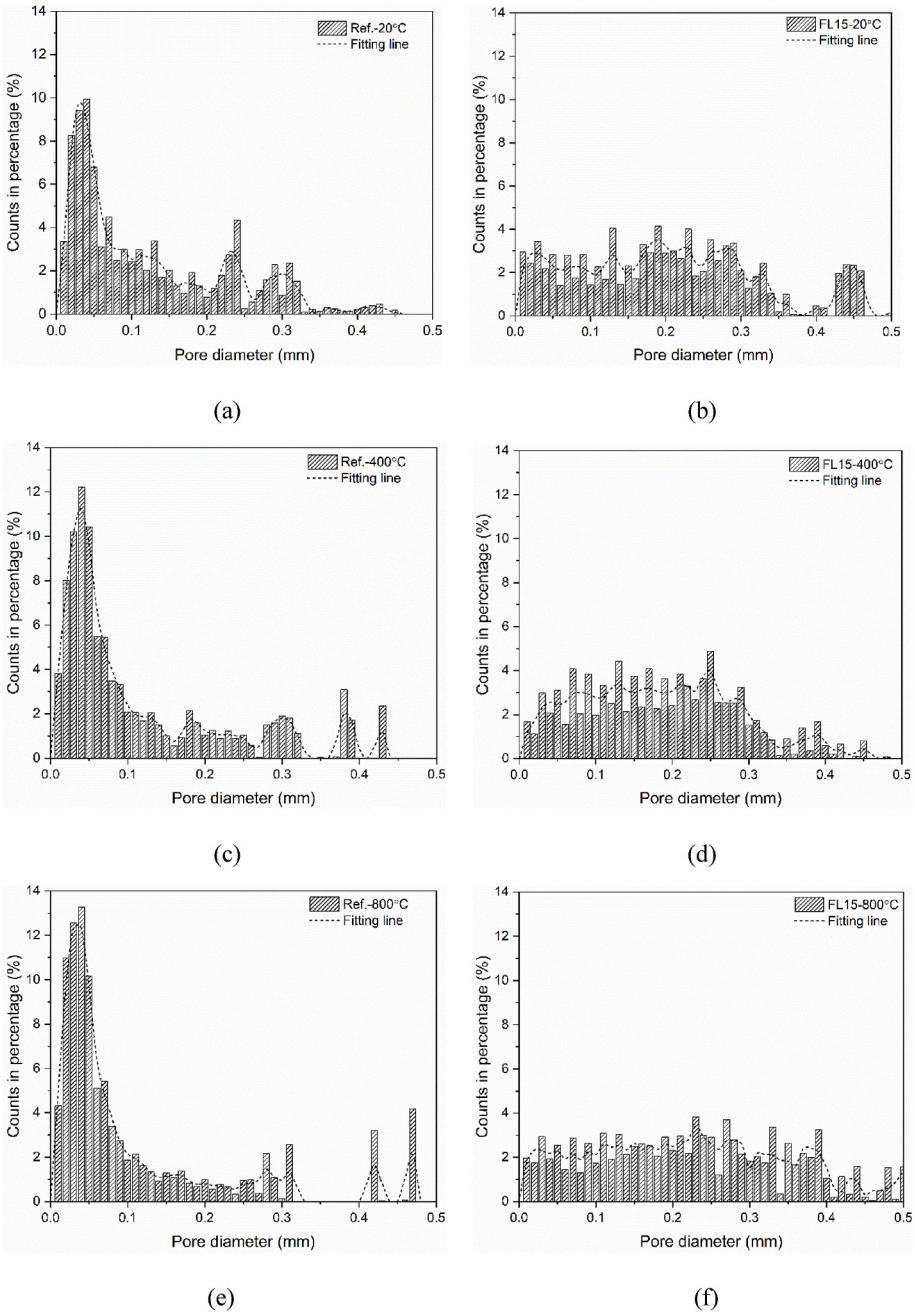

Fig. 11. Pore size distribution at different temperatures from Micro-CT: (a), (c), (e) Ref., (b), (d), (f) FL15.

system. However, in Wang et al. [65], the strength loss induced by conversion after 7 days is not detected with either cured in saturated limewater or higher alkali content (4%–8%). Similarly, Fernández-Carrasco et al. [38] and Pastor et al. [39] studied the hydration of CAC in a high alkaline environment and reported that the alkali media favours the conversion between calcium aluminate hydrates. As observed in the present study, the conversion reaction of LS occurs within 24 h with 8 M NaOH activation (Figs. 2 and 3). It can be concluded that the conversion rate of calcium aluminate hydrates is largely depending on the alkaline concentration and content, since a higher alkaline content results in a faster conversion reaction. In this case, the strength reduction phenomenon may occur earlier or even not be detectable with the presence of an alkali media.

The hydration reaction of LS is governed by different mechanisms with the presence of silica or pozzolan in the starting materials. For instance, it is suggested that in alkali activated LS with abundant soluble silica, the following reaction may take place [59]:

$$C_{12}A_7 + 51H + 6S \rightarrow 6C_2ASH_8(strätlingite) + AH_3$$

Similar results are also observed on alkali activation of CAC with a high content of reactive silica and/or low alkali content, the conversion is retarded since the metastable phases would transform into strätlingite instead of C_3AH_6 following the reactions [66,67]:

$$2CAH_{10} + S \rightarrow C_2ASH_8 + AH_3 + 9H \quad (5)$$

$$C_2AH_8 + S \rightarrow C_2ASH_8 \quad (6)$$

However, this is inconsistent with this work that no strätlingite is observed even with the highest LS substitution. Another case is reported by Fernández-Jiménez et al. [55] and Rivas Mercury et al. [68] on CAC system that with high alkali content and relatively low Si content or high temperature curing, a Si substituted phase $C_3AS_nH_m$ instead of

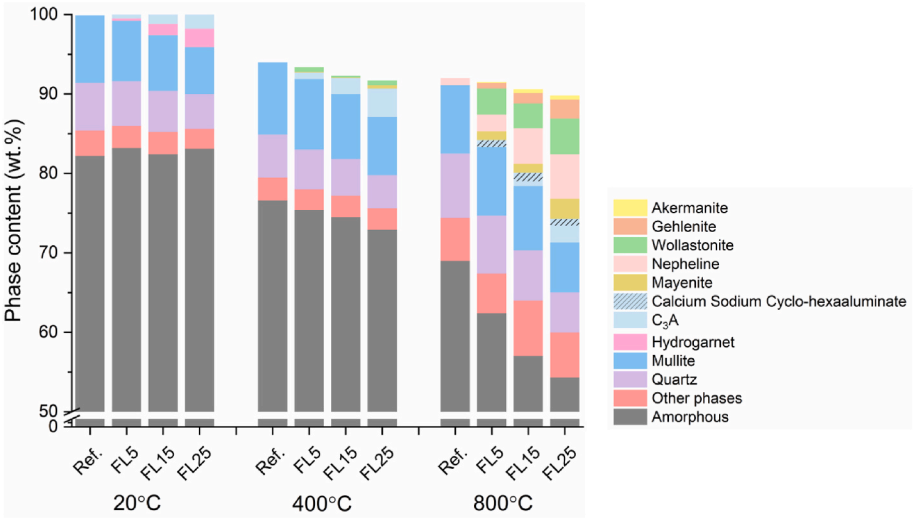

Fig. 12. Phase compositions of samples at different temperatures.

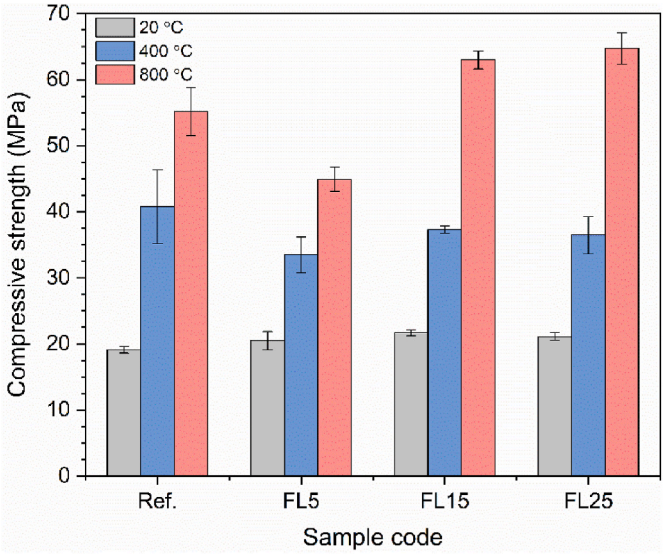

Fig. 13. Compressive strength of pastes exposed to different temperatures.

strätlingite is detected:

$$CA \xrightarrow{High\ OH^-} C_3AH_6 \tag{7}$$

$$C_3AH_6 \xrightarrow{Silicate} C_3AS_nH_m + \underset{(Amorphous\ and\ crystalline)}{Calcium\ aluminum\ silicate\ hydrate} \tag{8}$$

The results in the present work are more likely in accordance with the later situation. As shown in Table 7, the calcium aluminates and hydrates content in FL3 is determined by Rietveld analysis, in which 5.1 wt% of C_3A, 1.2 wt% of $C_{12}A_7$ and 2.8 wt% of C_3AH_6 are introduced by the raw LS, respectively. It is observed that C_3A decreases to 1.3 wt% at 28 d, and $C_{12}A_7$ is fully consumed after activation, indicating different degree of reactivity. While the stable hydrate of C_3AH_6 keeps decreasing from 2.8 wt% to 1.4 wt% after 28 d curing. The possible mechanism behind is, on the one hand, the high alkalinity with high temperature curing applied in the present work largely promotes the hydration of LS as well as the conversion reaction with the formation of C_3AH_6 at very early age. On the other hand, with the presence of silica provided by activator and fly ash, OH^- in C_3AH_6 is replaced by Si to form C-A-S-H phase following Eq. (8). Thus, in this work, strätlingite is not detected while C_3AH_6 is observed to decrease during the studied period. As a result, a continuous strength gain from 7 to 56 days is observed in all LS substituted pastes owing to the expedited conversion and formation of C-A-S-H phase. According to the discussion, the alkali activation of LS is similar to CAC and the reaction process is highly dependent on alkalinity, Si content and curing condition. A moderate alkalinity or high temperature curing can largely accelerate the conversion of metastable phase into stable phase, while the presence of Si can retard or prevent the conversion, and ultimately these conditions can avoid the strength reduction of LS incorporated pastes at later age.

Table 7
The variation of calcium aluminates and hydrates content in FL3 determined by XRD-Rietveld method (wt.%).

Phase	LS	St dev	7 d	St dev	28 d	St dev
C_3A	5.1	0.4	3.4	0.1	1.3	0.1
$C_{12}A_7$	1.2	0.2	0	0	0	0
C_3AH_6	2.8	0.2	2.6	0.2	1.4	0.1

4.2. *The influence of ladle slag on high temperature behavior of geopolymers*

As for blended Na_2O–CaO–Al_2O_3–SiO_2 system, with a sodium based alkali as the activator, Class F fly ash or metakaolin are often applied as the aluminosilicate source, while various secondary calcium sources can be found in previous works, for instance, cement, metallurgical slag, and lignite bottom ash [69–71]. The properties of secondary sources such as elemental composition, mineralogy, physical properties play a vital role on the performance of the resulting hybrid system [64,72–74]. Among these, GGBFS contains more than 40 wt% of calcium oxide and 30 wt% of silicon oxide in the reactive glass phase, which is the most commonly applied secondary source. Within an alkaline system, joint activation of FA and GGBFS results in formation of hybrid N–C-A-S-H gel, and typical slag based C-(A)-S-H products can be formed with higher dissolved Ca and Si concentrations. The formation of slag based products predominates the geopolymerization which not only largely accelerates the hydration degree but also impedes the formation of geopolymeric gel (N-A-S-H) [75]. Thus, a dense matrix is obtained with the coexistence of N–C-A-S-H and C-(A)-S-H products, and a relatively high initial mechanical strength can be achieved. However, as learned by our previous study [8], GGBFS has a negative impact on geopolymer based materials in terms of high temperature behavior. Firstly, the exchange of Na/Ca in aluminosilicate gel reduces the thermal stability of geopolymeric gel. Secondly, slag based products such as C–S–H gel are highly unstable at

elevated temperatures. Lastly, the compact matrix with low ductility is prone to failure under elevated temperatures due to thermal-induced stress. As a result, severe cracking, decomposition, and strength deterioration are always resulted after exposure to high temperatures.

LS contains similar chemical composition, especially calcium oxide content, in comparison to commonly used GGBFS. Nevertheless, it is found in this study that LS with high crystalline calcium and aluminium content exhibits a unique reaction process with the presence of alkali media and soluble Si, which shows a distinct influence on the hydration assemblage and microstructure of the hybrid geopolymer system. Owing to the prior weathering process, free lime is undetectable in LS (Table 4), and the majority of calcium and aluminium in LS is present in crystalline phases, namely tricalcium aluminate (C_3A) and mayenite ($C_{12}A_7$). In alkaline environment, the hydration and conversion of calcium aluminates is largely promoted to form calcium aluminate hydrates. With the continuous dissolution of Si from FA, the CAH phases convert into more stable C-A-S-H phase. In this case, the hydration is not significantly accelerated by adding LS, as evidenced by reaction heat release curve (Fig. 4). Moreover, the delayed formation of C-A-S-H gel might be unable or insufficient to alter the microstructure, and a loose matrix with a similar total porosity to sole FA based geopolymer is observed from MIP analysis (Table 5). In terms of aluminium content, it is learned from FT-IR (Fig. 6) that with a higher LS dosage, increased Al ions are introduced into Si–*O*-T tetrahedral within geopolymer gel, which contributes to the increased aluminosilicate species with a higher degree of cross-linking. The above results suggest that LS would not interfere geopolymerization process in contrast to GGBFS, and has a limited influence on the microstructural transformation within the studied substitution range.

The distinct influence of LS on the hydration of hybrid geopolymer system results in a different high temperature behavior from other blended geopolymers. A continuous strength gain at high temperatures is observed in this work (Fig. 13). This could be attributed to the synergistic effect of several characteristics such as microstructure and phase composition. For one thing, the loose matrix with homogenous pore size distribution in blended geopolymers helps to release the thermally induced water or gas vapour. Therefore, the inner thermal stress is reduced, and consequently, the inner pore structure is largely protected (see Table 5, Figs. 10, Fig. 11). For another, the addition of LS does not destroy the structure of thermally stable geopolymeric gel but contributes to a higher content of aluminosilicate species with the coexistence of N-A-S-H and C-A-S-H type gel. In this regard, the thermal stability of the hybrid binder gel is largely retained. Moreover, as learned from XRD Rietveld analysis in Fig. 12, more drastic recrystallization with the formation of thermally stable crystalline phases is observed at elevated temperatures with the increased LS substitution, which is likely to be another reason for the increased residual strength [64]. Here, it should be noted that the typical phase of nepheline that recrystallizes from N-A-S-H is increased with a higher LS substitution [76], which further proves that the incorporation of LS into geopolymer promotes the formation of geopolymeric gel, hence increases the thermal stability of binder gel.

5. Conclusions

This work investigates the hydration reaction and conversion process within the hybrid geopolymer system and verifies the possibility of utilizing ladle slag as a supplementary cementitious material in alkali activated material system for high temperature applications. Hybrid geopolymer pastes are prepared by substituting fly ash with ladle slag up to 25 wt% and its effect on reaction kinetics, hydration products, microstructure, and mechanical properties are investigated. Furthermore, the thermal behavior of hybrid geopolymers is evaluated based on phase transformation, structural change, and mechanical strength evolution at elevated temperatures. The following conclusions can be drawn:

- The dissolution, as well as polymerization within the hybrid system, is positively influenced by LS, as evidenced by a higher reaction heat intensity and cumulative heat release. The main hydration products within the hybrid system are C_3AH_6, C-A-S-H, and N-A-S-H type gels. The addition of LS promotes the hydration reaction, resulting in more hydration products, especially aluminosilicate gel, enabling a higher compressive strength.
- The strength deterioration of LS contained material at long term is avoided in hybrid geopolymer system. In an alkaline environment, the conversion reaction between metastable phases and stable C_3AH_6 is strongly expedited. With the presence of soluble silica, calcium aluminate hydrates absorb Si to form more stable C-A-S-H gel, which contributes to a continuous gain of compressive strength up to 56 days of curing. Nevertheless, the strength gain effect is lessened with more LS addition because of the limited provision of environmental silica, in addition to the adverse impact caused by the increased C_3AH_6 content.
- LS has no significant influence on the porosity of hybrid pastes within the present substitution level (i.e., 25 wt.%). Nevertheless, the addition of LS results in a wide and even pore size distribution pattern, which facilitates the release of inner water or gas vapour at elevated temperatures and thus contributes to better pore structural stability. However, increasing the LS substitution leads to a higher mass loss and volume shrinkage due to severer dehydration and recrystallization at high temperatures.
- The unique nature of LS with high crystalline calcium and aluminium content plays a vital role on high temperature behavior of hybrid geopolymer. The initially hydrated CAH phases in weathered LS transform into C-A-S-H, which protects the geopolymerization. As a result, the thermal stability of hybrid geopolymer is largely retained with the co-existence of N-A-S-H gel and C-A-S-H gel, enabling a continuous gain of compressive strength up to 800 °C. With more LS substitution, the residual strength, as well as strength gain rate after 800 °C, is increased thanks to the formation of thermally stable crystalline phases.

Declaration of competing interest

The authors declare that they have no known competing financial interests or personal relationships that could have appeared to influence the work reported in this paper.

Acknowledgements

This research is supported by China Scholarship Council (No. 201906370011) and the department of the Built Environment at Eindhoven University of Technology. The authors gratefully thank Prof. Dr. S.R. van der Laan (Tata Steel, The Netherlands) for the materials supply. Special thanks are given to Mr. Weitan Zhuang at Wuhan University (China) for his help with MIP measurements.

Appendix A. Supplementary data

Supplementary data to this article can be found online at https://doi.org/10.1016/j.cemconcomp.2022.104468.

References

[1] K.D. Hertz, Limits of spalling of fire-exposed concrete, Fire Saf. J. 38 (2003) 103–116, https://doi.org/10.1016/S0379-7112(02)00051-6.
[2] C. Alonso, L. Fernandez, Dehydration and rehydration processes of cement paste exposed to high temperature environments, J. Mater. Sci. 39 (2004) 3015–3024, https://doi.org/10.1023/B:JMSC.0000025827.65956.18.
[3] J.L. Provis, Geopolymers and other alkali activated materials: why, how, and what? Mater. Struct. 47 (2014) 11–25, https://doi.org/10.1617/s11527-013-0211-5.
[4] M. Lahoti, K.H. Tan, E.-H. Yang, A critical review of geopolymer properties for structural fire-resistance applications, Construct. Build. Mater. 221 (2019) 514–526, https://doi.org/10.1016/j.conbuildmat.2019.06.076.

[5] X. Gao, Q.L. Yu, H.J.H. Brouwers, Apply 29Si, 27Al MAS NMR and selective dissolution in identifying the reaction degree of alkali activated slag-fly ash composites, Ceram. Int. 43 (2017) 12408–12419, https://doi.org/10.1016/j.ceramint.2017.06.108.

[6] X. Gao, Q.L. Yu, A. Lazaro, H.J.H. Brouwers, Investigation on a green olivine nano-silica source based activator in alkali activated slag-fly ash blends: reaction kinetics, gel structure and carbon footprint, Cement Concr. Res. 100 (2017) 129–139, https://doi.org/10.1016/j.cemconres.2017.06.007.

[7] A. Rafeet, R. Vinai, M. Soutsos, W. Sha, Effects of slag substitution on physical and mechanical properties of fly ash-based alkali activated binders (AABs), Cem, Concr. Res. 122 (2019) 118–135, https://doi.org/10.1016/j.cemconres.2019.05.003.

[8] Y. Luo, S.H. Li, K.M. Klima, H.J.H. Brouwers, Q. Yu, Degradation mechanism of hybrid fly ash/slag based geopolymers exposed to elevated temperatures, Cement Concr. Res. 151 (2022), 106649, https://doi.org/10.1016/j.cemconres.2021.106649.

[9] N.K. Lee, K.T. Koh, G.H. An, G.S. Ryu, Influence of binder composition on the gel structure in alkali activated fly ash/slag pastes exposed to elevated temperatures, Ceram. Int. 43 (2017) 2471–2480, https://doi.org/10.1016/j.ceramint.2016.11.042.

[10] Z. Pan, Z. Tao, Y.F. Cao, R. Wuhrer, T. Murphy, Compressive strength and microstructure of alkali-activated fly ash/slag binders at high temperature, Cement Concr. Compos. 86 (2018) 9–18, https://doi.org/10.1016/j.cemconcomp.2017.09.011.

[11] S. Kourounis, S. Tsivilis, P.E. Tsakiridis, G.D. Papadimitriou, Z. Tsibouki, Properties and hydration of blended cements with steelmaking slag, Cement Concr. Res. 37 (2007) 815–822, https://doi.org/10.1016/j.cemconres.2007.03.008.

[12] E. Adesanya, K. Ohenoja, P. Kinnunen, M. Illikainen, Alkali activation of ladle slag from steel-making process, J. Sustain. Metall. 3 (2017) 300–310, https://doi.org/10.1007/s40831-016-0089-x.

[13] V.Z. Serjun, B. Mirti, A. Mladenovi, Evaluation of ladle slag as a ptential material for building and civil engineering, Mater. Tehnol. (2013) 8.

[14] D. Adolfsson, R. Robinson, F. Engström, B. Björkman, Influence of mineralogy on the hydraulic properties of ladle slag, Cement Concr. Res. 41 (2011) 865–871, https://doi.org/10.1016/j.cemconres.2011.04.003.

[15] M.C. Bignozzi, S. Manzi, I. Lancellotti, E. Kamseu, L. Barbieri, C. Leonelli, Mix-design and characterization of alkali activated materials based on metakaolin and ladle slag, Appl. Clay Sci. 73 (2013) 78–85, https://doi.org/10.1016/j.clay.2012.09.015.

[16] H.G. Midgley, A. Midgley, The conversion of high alumina cement, Mag. Concr. Res. (2015), https://doi.org/10.1680/macr.1975.27.91.59.

[17] T. Matusinović, J. Šipušić, N. Vrbos, Porosity–strength relation in calcium aluminate cement pastes, Cement Concr. Res. 33 (2003) 1801–1806, https://doi.org/10.1016/S0008-8846(03)00201-1.

[18] V. Ducman, A. Mladenovič, The potential use of steel slag in refractory concrete, Mater. Char. 62 (2011) 716–723, https://doi.org/10.1016/j.matchar.2011.04.016.

[19] D. Torréns-Martín, L. Fernández-Carrasco, S. Martínez-Ramírez, Hydration of calcium aluminates and calcium sulfoaluminate studied by Raman spectroscopy, Cement Concr. Res. 47 (2013) 43–50, https://doi.org/10.1016/j.cemconres.2013.01.015.

[20] K.L. Scrivener, J.-L. Cabiron, R. Letourneux, High-performance concretes from calcium aluminate cements, Cement Concr. Res. 29 (1999) 1215–1223, https://doi.org/10.1016/S0008-8846(99)00103-9.

[21] E. Adesanya, M. Karhu, A. Ismailov, K. Ohenoja, P. Kinnunen, M. Illikainen, Thermal behaviour of ladle slag mortars containing ferrochrome slag aggregates, Adv. Cement Res. 33 (2021) 168–182, https://doi.org/10.1680/jadcr.19.00040.

[22] A. Natali Murri, W.D.A. Rickard, M.C. Bignozzi, A. van Riessen, High temperature behaviour of ambient cured alkali-activated materials based on ladle slag, Cement Concr. Res. 43 (2013) 51–61, https://doi.org/10.1016/j.cemconres.2012.09.011.

[23] British Standards Institution: London, BS EN 1015-3 : Methods of Test for Mortar for Masonry - Part 3: Determination of Consistence of Fresh Mortar (By Flow Table), 1999.

[24] T. Williamson, M.C.G. Juenger, The role of activating solution concentration on alkali–silica reaction in alkali-activated fly ash concrete, Cement Concr. Res. 83 (2016) 124–130, https://doi.org/10.1016/j.cemconres.2016.02.008.

[25] A. Fernández-Jiménez, Á. Palomo, T. Vazquez, R. Vallepu, T. Terai, K. Ikeda, Alkaline activation of blends of metakaolin and calcium aluminate, J. Am. Ceram. Soc. 91 (2008) 1231–1236, https://doi.org/10.1111/j.1551-2916.2007.02002.x.

[26] British Standards Institution: London, Methods of Testing Cement. Part 1, Part 1, 2016.

[27] J. Pommersheim, J. Chang, Kinetics of hydration of tricalcium aluminate, Cement Concr. Res. 16 (1986) 440–450, https://doi.org/10.1016/0008-8846(86)90120-1.

[28] A.J. Majumbar, B. Singh, R.N. Edmonds, Hydration of mixtures of C12A7 and granulated blastfurnace slag, Cement Concr. Res. 19 (1989) 848–856, https://doi.org/10.1016/0008-8846(89)90097-5.

[29] W.A. Corstanje, H.N. Stein, J.M. Stevels, Hydration reactions in pastes C3S+C3A+CaSO4.2aq+H2O at 25°C.I, Cem, Concr. Res. 3 (1973) 791–806, https://doi.org/10.1016/0008-8846(73)90012-4.

[30] J. Setién, D. Hernández, J.J. González, Characterization of ladle furnace basic slag for use as a construction material, Construct. Build. Mater. 23 (2009) 1788–1794, https://doi.org/10.1016/j.conbuildmat.2008.10.003.

[31] E. Adesanya, H. Sreenivasan, A.M. Kantola, V.-V. Telkki, K. Ohenoja, P. Kinnunen, M. Illikainen, Ladle slag cement – characterization of hydration and conversion, Construct. Build. Mater. 193 (2018) 128–134, https://doi.org/10.1016/j.conbuildmat.2018.10.179.

[32] N. Ukrainczyk, T. Matusinovic, S. Kurajica, B. Zimmermann, J. Sipusic, Dehydration of a layered double hydroxide—C2AH8, Thermochim. Acta 464 (2007) 7–15, https://doi.org/10.1016/j.tca.2007.07.022.

[33] S.M. Bushnell-Watson, J.H. Sharp, The application of thermal analysis to the hydration and conversión Reactions of calcium alumínate Cements, Mater. Construcción 42 (1992) 13–32, https://doi.org/10.3989/mc.1992.v42.i228.694.

[34] E. Nonnet, N. Lequeux, P. Boch, Elastic properties of high alumina cement castables from room temperature to 1600°C, J. Eur. Ceram. Soc. 19 (1999) 1575–1583, https://doi.org/10.1016/S0955-2219(98)00255-6.

[35] B. Yuan, Q.L. Yu, H.J.H. Brouwers, Assessing the chemical involvement of limestone powder in sodium carbonate activated slag, Mater. Struct. 50 (2017) 136, https://doi.org/10.1617/s11527-017-1003-0.

[36] K. Rozov, U. Berner, C. Taviot-Gueho, F. Leroux, G. Renaudin, D. Kulik, L. W. Diamond, Synthesis and characterization of the LDH hydrotalcite–pyroaurite solid-solution series, Cement Concr. Res. 40 (2010) 1248–1254, https://doi.org/10.1016/j.cemconres.2009.08.031.

[37] N. Ukrainczyk, T. Matusinovic, S. Kurajica, B. Zimmermann, J. Sipusic, Dehydration of a layered double hydroxide—C2AH8, Thermochim. Acta 464 (2007) 7–15, https://doi.org/10.1016/j.tca.2007.07.022.

[38] L. Fernández-Carrasco, M.T. Blanco-Varela, F. Puertas, T. Vázquez, F.P. Glasser, E. Lachowski, Hydration of high alumina cement in the presence of alkalis, Adv. Cement Res. 12 (2000) 143–152, https://doi.org/10.1680/adcr.2000.12.4.143.

[39] C. Pastor, A. Fernández-Jiménez, T. Vázquez, Á. Palomo, Calcium aluminate cement hydration in a high alkalinity environment, Mater. Construcción 59 (2009) 21–34, https://doi.org/10.3989/mc.2009.42407.

[40] S.A. Bernal, J.L. Provis, V. Rose, R. Mejía de Gutierrez, Evolution of binder structure in sodium silicate-activated slag-metakaolin blends, Cement Concr. Compos. 33 (2011) 46–54, https://doi.org/10.1016/j.cemconcomp.2010.09.004.

[41] Z. Sun, A. Vollpracht, Isothermal calorimetry and in-situ XRD study of the NaOH activated fly ash, metakaolin and slag, Cement Concr. Res. 103 (2018) 110–122, https://doi.org/10.1016/j.cemconres.2017.10.004.

[42] S. Chithiraputhiran, N. Neithalath, Isothermal reaction kinetics and temperature dependence of alkali activation of slag, fly ash and their blends, Construct. Build. Mater. 45 (2013) 233–242, https://doi.org/10.1016/j.conbuildmat.2013.03.061.

[43] C. Jiang, A. Wang, X. Bao, T. Ni, J. Ling, A review on geopolymer in potential coating application: materials, preparation and basic properties, J. Build. Eng. 32 (2020), 101734, https://doi.org/10.1016/j.jobe.2020.101734.

[44] A. Fernández-Jiménez, A. Palomo, Mid-infrared spectroscopic studies of alkali-activated fly ash structure, Microporous Mesoporous Mater. 86 (2005) 207–214, https://doi.org/10.1016/j.micromeso.2005.05.057.

[45] S. Ashrit, R.V. Chatti, S. Sarkar, R. Venugopal, U.G. Nair, An infrared spectroscopic study of non-metallic portion of Linz-Donawitz slag fines generated at Tata Steel, Jamshedpur, Metall. Res. Technol. 115 (2018) 608, https://doi.org/10.1051/metal/2018024.

[46] R.A. Schroeder, L.L. Lyons, Infra-red spectra of the crystalline inorganic aluminates, J. Inorg. Nucl. Chem. 28 (1966) 1155–1163, https://doi.org/10.1016/0022-1902(66)80441-4.

[47] J.F. Zapata, M. Gomez, H.A. Colorado, Structure-property relation and Weibull analysis of calcium aluminate cement pastes, Mater. Char. 134 (2017) 9–17, https://doi.org/10.1016/j.matchar.2017.10.010.

[48] S. Maitra, S. Bose, N. Bandyopadhyay, A. Roychoudhury, Dehydration kinetics of calcium aluminate cement hydrate under non-isothermal conditions, Ceram. Int. 31 (2005) 371–374, https://doi.org/10.1016/j.ceramint.2004.06.002.

[49] M.A. Soleimani, R. Naghizadeh, A. Mirhabibi, F. Golestanifard, The influence of phosphorus slag addition on microstructure and mechanical properties of metakaolin-based geopolymer pastes, Ceram. - Silik. 57 (2013) 33–38.

[50] E.N. Kani, H. Mehdizadeh, Investigating gel molecular structure and its relation with mechanical strength in geopolymer cement based on natural pozzolan using in situ ATR-FTIR spectroscopy, J. Mater. Civ. Eng. 29 (2017), 04017078, https://doi.org/10.1061/(ASCE)MT.1943-5533.0001917.

[51] L. Alarcon-Ruiz, G. Platret, E. Massieu, A. Ehrlacher, The use of thermal analysis in assessing the effect of temperature on a cement paste, Cement Concr. Res. 35 (2005) 609–613, https://doi.org/10.1016/j.cemconres.2004.06.015.

[52] J. Payá, J. Monzó, M.V. Borrachero, E. Perris, F. Amahjour, Thermogravimetric methods for determining carbon content in fly ashes, Cement Concr. Res. 28 (1998) 675–686, https://doi.org/10.1016/S0008-8846(98)00030-1.

[53] X. Gao, Q.L. Yu, H.J.H. Brouwers, Reaction kinetics, gel character and strength of ambient temperature cured alkali activated slag–fly ash blends, Construct. Build. Mater. 80 (2015) 105–115, https://doi.org/10.1016/j.conbuildmat.2015.01.065.

[54] I. Ismail, S.A. Bernal, J.L. Provis, R. San Nicolas, S. Hamdan, J.S.J. van Deventer, Modification of phase evolution in alkali-activated blast furnace slag by the incorporation of fly ash, Cement Concr. Compos. 45 (2014) 125–135, https://doi.org/10.1016/j.cemconcomp.2013.09.006.

[55] A. Fernández-Jiménez, T. Vázquez, A. Palomo, Effect of sodium silicate on calcium aluminate cement hydration in highly alkaline media: a microstructural characterization, J. Am. Ceram. Soc. 94 (2011) 1297–1303, https://doi.org/10.1111/j.1551-2916.2010.04242.x.

[56] L. Li, W. Liu, Q. You, M. Chen, Q. Zeng, C. Zhou, M. Zhang, Relationships between microstructure and transport properties in mortar containing recycled ceramic powder, J. Clean. Prod. 263 (2020), 121384, https://doi.org/10.1016/j.jclepro.2020.121384.

[57] S. Choi, J.-M. Kim, D. Han, J.-H. Kim, Hydration properties of ladle furnace slag powder rapidly cooled by air, Construct. Build. Mater. 113 (2016) 682–690, https://doi.org/10.1016/j.conbuildmat.2016.03.089.

[58] Concrete: Microstructure, Properties, and Materials, McGraw-Hill Professional., Indian Concrete Institute, 2014.

[59] E. Adesanya, K. Ohenoja, P. Kinnunen, M. Illikainen, Properties and durability of alkali-activated ladle slag, Mater. Struct. 50 (2017) 255, https://doi.org/10.1617/s11527-017-1125-4.
[60] A.M. Kaja, K. Schollbach, S. Melzer, S.R. van der Laan, H.J.H. Brouwers, Q. Yu, Hydration of potassium citrate-activated BOF slag, Cement Concr. Res. 140 (2021), 106291, https://doi.org/10.1016/j.cemconres.2020.106291.
[61] M. Lahoti, S.F. Wijaya, K.H. Tan, E.-H. Yang, Tailoring sodium-based fly ash geopolymers with variegated thermal performance, Cement Concr. Compos. 107 (2020), 103507, https://doi.org/10.1016/j.cemconcomp.2019.103507.
[62] M. Lahoti, K.K. Wong, K.H. Tan, E.-H. Yang, Effect of alkali cation type on strength endurance of fly ash geopolymers subject to high temperature exposure, Mater. Des. 154 (2018) 8–19, https://doi.org/10.1016/j.matdes.2018.05.023.
[63] A. Van Riessen, W. Rickard, J. Sanjayan, 15 - thermal properties of geopolymers, in: J.L. Provis, J.S.J. van Deventer (Eds.), Geopolymers, Woodhead Publishing, 2009, pp. 315–342, https://doi.org/10.1533/9781845696382.2.315.
[64] K. Dombrowski, A. Buchwald, M. Weil, The influence of calcium content on the structure and thermal performance of fly ash based geopolymers, J. Mater. Sci. 42 (2007) 3033–3043, https://doi.org/10.1007/s10853-006-0532-7.
[65] W.-C. Wang, H.-Y. Wang, H.-C. Tsai, Study on engineering properties of alkali-activated ladle furnace slag geopolymer, Construct. Build. Mater. 123 (2016) 800–805, https://doi.org/10.1016/j.conbuildmat.2016.07.068.
[66] N.Y. Mostafa, Z.I. Zaki, O.H. Abd Elkader, Chemical activation of calcium aluminate cement composites cured at elevated temperature, Cement Concr. Compos. 34 (2012) 1187–1193, https://doi.org/10.1016/j.cemconcomp.2012.08.002.
[67] J. Ding, Y. Fu, J.J. Beaudoin, Study of hydration mechanisms in the high alumina cement - sodium silicate system, Cement Concr. Res. 26 (1996) 799–804, https://doi.org/10.1016/S0008-8846(96)85017-4.
[68] J.M. Rivas Mercury, X. Turrillas, A.H. de Aza, P. Pena, Calcium aluminates hydration in presence of amorphous SiO2 at temperatures below 90°C, J. Solid State Chem. 179 (2006) 2988–2997, https://doi.org/10.1016/j.jssc.2006.05.017.
[69] C. Shi, D. Roy, P. Krivenko, Alkali-Activated Cements and Concretes, CRC Press, London, 2014, https://doi.org/10.1201/9781482266900.
[70] M. Frias, J. Cabrera, Influence of MK on the reaction kinetics in MK/lime and MK-blended cement systems at 20°C, Cement Concr. Res. 31 (2001) 519–527, https://doi.org/10.1016/S0008-8846(00)00465-8.
[71] E. ul Haq, S. Kunjalukkal Padmanabhan, A. Licciulli, Synthesis and characteristics of fly ash and bottom ash based geopolymers–A comparative study, Ceram. Int. 40 (2014) 2965–2971, https://doi.org/10.1016/j.ceramint.2013.10.012.
[72] C.K. Yip, G.C. Lukey, J.S.J. van Deventer, The coexistence of geopolymeric gel and calcium silicate hydrate at the early stage of alkaline activation, Cement Concr. Res. 35 (2005) 1688–1697, https://doi.org/10.1016/j.cemconres.2004.10.042.
[73] S. Alonso, A. Palomo, Calorimetric study of alkaline activation of calcium hydroxide–metakaolin solid mixtures, Cement Concr. Res. 31 (2001) 25–30, https://doi.org/10.1016/S0008-8846(00)00435-X.
[74] J. Cabrera, M.F. Rojas, Mechanism of hydration of the metakaolin–lime–water system, Cement Concr. Res. 31 (2001) 177–182, https://doi.org/10.1016/S0008-8846(00)00456-7.
[75] X.Y. Zhuang, L. Chen, S. Komarneni, C.H. Zhou, D.S. Tong, H.M. Yang, W.H. Yu, H. Wang, Fly ash-based geopolymer: clean production, properties and applications, J. Clean. Prod. 125 (2016) 253–267, https://doi.org/10.1016/j.jclepro.2016.03.019.
[76] S.M. Park, J.G. Jang, N.K. Lee, H.K. Lee, Physicochemical properties of binder gel in alkali-activated fly ash/slag exposed to high temperatures, Cement Concr. Res. 89 (2016) 72–79, https://doi.org/10.1016/j.cemconres.2016.08.004.